RMetS
Royal Meteorological Society

Deconstructing the Hadley cell heat transport

C. Heaviside* and A. Czaja
Department of Physics, Imperial College, London, United Kingdom

*Correspondence to: C. Heaviside, Centre for Radiation, Chemical and Environmental Hazards, Health Protection Agency, Chilton, Didcot, Oxon, OX11 0RQ, UK. E-mail: clare.heaviside05@imperial.ac.uk

The mechanisms responsible for poleward atmospheric heat transport at low latitudes are examined in the European Centre for Medium-Range Weather Forecasts (ECMWF) Re-Analysis (ERA-40) dataset. Deep meridional overturning circulations are found in regions experiencing frequent convection (i.e. the Indo-Pacific 'warm pool') and it is suggested that these are the primary reason why atmospheric heat transport seems dominated by axisymmetric motions or 'Hadley cell heat transport'. In contrast, the more complex distribution of meridional mass transport by the circulations over the 'cold tongue' regions (such as the eastern Atlantic area) and the presence of a pronounced minimum in moist static energy at mid-levels constrain these regions to contribute little to poleward heat transport year round. Regions experiencing frequent convection do not, however, account for all the *annual mean* poleward atmospheric heat transport. At the Equator, an annual net southward transport of heat of about 0.4 PW (1 PW = 10^{15} W) is found, but the deep overturning cells found in the most convectively active regions contribute only 25% of this. This small contribution of $\sim$0.1 PW is understood to reflect a seasonal cancellation between large ($\sim$1 PW) northward and southward heat transports in boreal winter and summer respectively. During December-February, most of the cross-equatorial heat transport is attributable to the convective regions, whereas in June-August, only half is attributable to these regions. In this season, there is a significant amount of heat transport by the strong Somali jet associated with the Asian summer monsoon. Rather than attributing the net southward cross-equatorial heat transport to asymmetries in the climatology associated with the northerly position of the intertropical convection zones throughout the year over the eastern Pacific and Atlantic oceans, our diagnostics suggest that the Somali jet is a significant contributor to the annual net southward atmospheric heat transport at the Equator. **Copyright © 2012 Royal Meteorological Society**

Key Words: Hadley cell; heat transport; tropics; atmospheric circulation; moist static energy; monsoon; convection.

Received 6 January 2012; Revised 12 October 2012; Accepted 1 November 2012; Published online in Wiley Online Library

Citation: Heaviside C, Czaja A. 2012. Deconstructing the Hadley cell heat transport. *Q. J. R. Meteorol. Soc.* DOI:10.1002/qj.2085

1. Introduction

Heat transport from low to high latitudes in the atmosphere is achieved by a wide range of processes. In midlatitudes, travelling and stationary waves are believed to be the main carrier of heat across latitude circles. This is in sharp contrast to low latitudes where axisymmetric motions are invoked as the main mechanism for poleward heat transport (see figure 13.11 in Peixoto and Oort (1992)). Such a two-dimensional view of the tropical atmosphere is often proposed as the simplest possible description, and conceptual models of the interaction of the ocean

and the atmosphere are based on it. For example, Held (2001) expresses the contribution of time mean motions to atmospheric heat transport as:

$$H_{\mathrm{A}} = \psi_{\mathrm{A}} \Delta h \tag{1}$$

in which ψ_{A} is the strength of the overturning (Hadley) cell in the meridional plane and Δh is the energy contrast between the poleward and equatorward branches of the circulation.

To some extent it is difficult to convince oneself for such a dominance of two-dimensional mechanisms at low latitudes. Indeed, the zonal distribution of temperature at the sea surface varies by 5–10 K depending on the extent of the cold tongue regions (Philander, 1990), and the zonal distribution of moisture (or latent heat) is very non-uniform, reflecting the coexistence of regions experiencing frequent convection and moistening with regions experiencing the compensating subsidence and associated drying. El Niño events act to expel those zonal asymmetries and bring the tropical atmosphere closer to an axisymmetric state (Oort and Yienger, 1996). In an analysis of global oceanic and atmospheric heat transport, Czaja and Marshall (2006) noted that at all latitudes, the equatorward mass transport by the atmosphere occurs within layers with moist static energy lower than the zonally averaged value. If this result was expected in midlatitudes due to the presence of cold air outbreaks (Held and Schneider, 1999), it is more surprising in the tropics. A possible explanation could lie in the fact that at low latitudes, low-level equatorward flow often occurs over the cold tongues of the Atlantic and Pacific oceans.

The fact that Eq. (1) can be used to give a good approximation of the poleward atmospheric heat transport despite such spatial variability in tropical climatology could be understood if the heat transport were dominated by a 'true' overturning circulation in one region of the tropics. By this, it is meant a longitudinal sector where northward and southward mass transports balance and take the form of a simple dipole in the vertical. This type of mass transport is indeed predicted in regions experiencing convection frequently, under the assumption that the atmosphere is neutral to upward displacement of air parcels lifted reversibly from the surface (Emanuel *et al.*, 1994). This overturning circulation is also the classic response of the atmosphere to heating predicted in the linear shallow-water model of Gill (1980). It is the purpose of this study to test if these regions indeed dominate the zonally averaged atmospheric heat transport by analysing in detail the structure of the poleward and equatorward mass fluxes as a function of longitude in the tropics. To capture the largest meridional mass transports we will focus on the Equator because this is where mass transport is at a maximum during the solstitial seasons (Dima and Wallace, 2003).

Another reason for focusing on the Equator is that several climatologies have revealed a net southward atmospheric heat transport across the Equator, despite the fact that the sum of oceanic and atmospheric cross-equatorial heat transport cannot be distinguished from zero (Trenberth and Caron, 2001; Wunsch, 2005). This suggests that some form of compensation between oceanic and atmospheric transport is taking place in the deep tropics. It is hoped that by better understanding the mechanisms controlling cross-equatorial atmospheric heat transport it will be possible to move forward in our understanding of this intriguing compensation, or make the case that it is coincidental.

The article is structured as follows. In section 2 we present zonal sections of meridional winds and moist static energy at the Equator from a 10-year reanalysis dataset. The associated meridional mass transport is then studied in section 3 by sorting as a function of surface moist static energy. This new diagnostic provides a simple view of the mechanisms responsible for atmospheric heat transport across the Equator, the latter being addressed directly in section 4. Conclusions are drawn in section 5.

2. Zonal and vertical variations of moist static energy and meridional winds at the Equator

2.1. General considerations

The total amount of energy carried by an air parcel of unit mass is the moist static energy (h), defined as $C_{\mathrm{p}}T + L_{\mathrm{v}}q + gz$, where C_{p} is the specific heat capacity of air at constant pressure, T is air temperature, L_{v} is the latent heat of vaporization, q is specific humidity and gz is geopotential (Gill, 1982; Neelin and Held, 1987). At the surface (denoted by subscript sfc) moist static energy simplifies to:

$$h_{\mathrm{sfc}} = C_{\mathrm{p}}T_{\mathrm{sfc}} + L_{\mathrm{v}}q_{\mathrm{sfc}} \tag{2}$$

because the geopotential term vanishes at $z = 0$. Furthermore, to the extent that relative humidity remains fairly uniform near the surface (which is certainly true for the open ocean), h_{sfc} is in practice a function of temperature only, because the saturation specific humidity varies little with pressure. Spatial variations in surface temperature, arising from ocean currents and land–sea contrast are thus expected to act as sources of moist static energy contrasts.

Sufficiently high up in the troposphere, the moisture term vanishes and moist static energy reduces to dry static energy ($C_{\mathrm{p}}T + gz$). At the Equator, where the Coriolis parameter vanishes, very large winds would result from gradients in dry static energy (or Montgomery potential) and in effect, this dynamical constraint forces the temperature and geopotential fields to be fairly homogeneous above the boundary layer (Wallace, 1992). As a result, very weak horizontal variations in moist static energy are expected in the upper atmosphere at the Equator (see e.g. Polvani and Sobel, (2002) for more theoretical motivation on this topic). For the layer sandwiched between the boundary layer and the upper atmosphere, horizontal variations in moist static energy will reflect primarily those in moisture content.

In convective regions of the tropical atmosphere, which usually coincide with high sea-surface temperature (SST) and, from Eq. (2), to high surface moist static energy, moist convection acts to maintain a moist adiabatic temperature profile throughout the troposphere (Xu and Emanuel, 1989). This in turn limits the vertical variations in moist static energy because saturation entropy (constant in a moist adiabatic process) and moist static energy are closely linked (e.g. Bohren and Albrecht, 1998).

From these considerations, we would expect h to be relatively uniform horizontally at upper levels and to vary more in the horizontal at lower levels, as a result of variations in temperature and moisture in the boundary layer. In the vertical, we would expect strongly convecting regions, often over the warmest parts of the ocean, to have approximately constant h with height and high relative humidity. Over cooler sea surfaces, we would expect less convection and

larger vertical variations in h. In these drier regions, air is often descending from convective regions, and can lead to a minimum in h and relative humidity at mid-tropospheric (around 600 hPa) levels (e.g. Emanuel *et al.*, 1994).

2.2. Data

The data used for the analysis came from the ERA-40 reanalysis dataset of the European Centre for Medium-Range Weather Forecasting (Uppala *et al.*, 2005). See Trenberth *et al.* (2001) for an overview of reanalysis data in the tropics. The ERA-40 dataset describes the state of the atmosphere from 1957 to 2001 and combines a physical model with observations in order to create a global reanalysis product of various meteorological variables (Uppala *et al.*, 2005). Ten years (1992–2001) of monthly mean data were used to calculate seasonal means for each of the years (DJF, MAM, JJA and SON represent December to February, March to May, June to August and September to November, respectively) and the mean was taken over 10 years for each season. We used data at 13 pressure levels: 1000, 925, 850, 775, 700, 600, 500, 400, 300, 250, 200, 150 and 100 hPa with a horizontal resolution of $1^\circ \times 1^\circ$. Variables used included meridional wind, temperature, relative humidity, geopotential height and surface pressure.

2.3. Seasonal variability

The distribution of h and meridional winds throughout the troposphere at the Equator for the seasons DJF and JJA is shown in Figure 1. White areas at the surface represent the grid points occupied by land. Since the section is taken along the Equator, Africa coincides with around 10°–45° of longitude, Indonesia with 100°–135° and South America with 280°–310°. The value of h has been divided by C_P in order to give units in Kelvin.

For both JJA and DJF, moist static energy (in colour online) shows little horizontal variation above around 300 hPa, whereas horizontal gradients are larger near the surface, which is expected based on the discussion in section 2.1. There is a minimum in h at around 600 hPa. Over the lower SSTs, such as those in the eastern Pacific, the minimum in h extends down further towards the surface than in other regions. The Pacific warm pool has relatively high values of h_{sfc} compared with that of the eastern Pacific and Atlantic oceans. In fact, horizontal gradients in h_{sfc} between parts of the tropics at the Equator are of the same order as vertical gradients. Between the regions with warmest and coldest sea surfaces, the difference in h_{sfc} can be as large as 15 K. There is also less of a pronounced minimum of h at mid-levels in places where h_{sfc} is high.

2.3.1. June–August

During JJA (Figure 1, bottom panel), the general structure of the flow is northward at low levels and southward at upper levels, consistent with a cross-section through an overturning Hadley cell with an ascending branch in the Northern Hemisphere, although there is some departure from this structure in regions where h_{sfc} is low. The southward flow is confined mainly to above 400 hPa, where h is higher than the lower level northward flow, resulting in a net southward transport of heat.

Above the eastern Pacific and Atlantic oceans, the structure of the flow differs from that of other regions and strong surface northward winds are observed below 750 hPa. There is also a low level southward return flow centred at around 600 hPa, where moist static energy is at a minimum, reflecting regions of descending dry air. Above this is a small region of northward flow at around 400 hPa. The Hadley cell is acting to transport heat from the Northern to the Southern Hemisphere during JJA, although in the regions where h_{sfc} is low, the flow at 600 hPa acts to transport *low* energy air from north to south, which opposes the direction of the main Hadley cell heat transport. Over the Indian Ocean, the flow is strongly northward flowing, with mean winds reaching 13 m s^{-1} along the coast of Somalia. Over the western part of the Indian Ocean, there is little return flow at upper levels, with the main southward flow to the west and east of the region containing the Somali jet, which is associated with the Indian monsoon.

2.3.2. December–February

The circulation in DJF is generally a reversal of JJA, because now the ascending branch of the Hadley cell is in the Southern Hemisphere and the direction of the mean heat transport is from the Southern to Northern Hemisphere (Figure 1, top panel). The cold tongue is less well developed during DJF compared with JJA, and the minimum in h does not extend as far down to the surface. There is still northward flow at the surface over the eastern Pacific and Atlantic oceans, because the intertropical convergence zone (ITCZ) is north of the Equator in these areas throughout the year (Philander *et al.*, 1996), although it is weaker than in JJA. In fact in some parts of these colder, drier regions, the direction of the flow reverses up to three times. Again it could be that this more complicated flow opposes the general direction of Hadley cell heat transport. Aside from the more complex regions, there is mainly southward flow below 500 hPa, with some northward flowing winds just above the surface in the eastern Pacific and Atlantic. The situation over the Indian Ocean shows a reversal in direction, reflecting the reversal of the monsoon circulation, with surface winds flowing southward during DJF, and a less intense flow along the western side. Due to the less pronounced low in h over the eastern Pacific and Atlantic during DJF compared with JJA, horizontal gradients in moist static energy at the surface are slightly reduced but still can be as large as 9 K.

3. Mass transport as a function of surface moist static energy

3.1. Framework of analysis

We propose a framework that enables us to view the circulation of the atmosphere as a function of low-level moist static energy (h_{sfc}) rather than latitude or longitude. Other work has sorted variables in ways other than by geography: one such example is that of Bony *et al.* (2004), which uses a framework based on the large-scale atmospheric circulation to define a series of dynamical regimes responding to different values of vertical velocity (ω). In addition, mass flux traditionally has been examined on pressure levels, but also within dry (Held and Schneider, 1999) and moist isentropic layers (Pauluis *et al.*, 2008), in an attempt to capture a more Lagrangian description of the circulation.

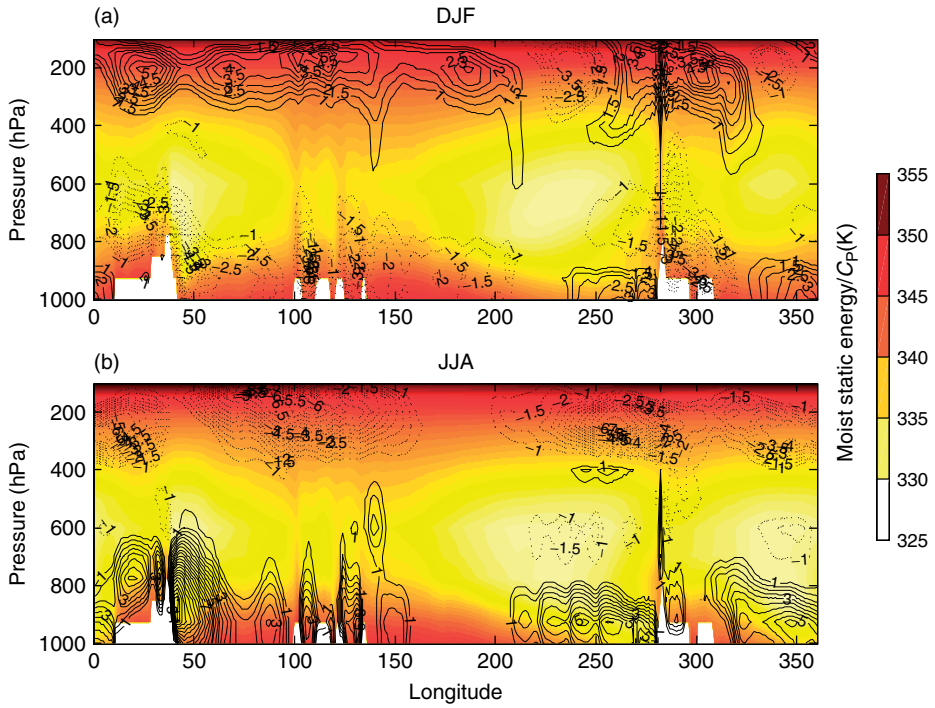

Figure 1. Moist static energy (shading: colours online) in K and meridional winds (contours) in m s^{-1} at the Equator for (a) DJF and (b) JJA, 1992–2001. Positive (solid) contours show northward winds and negative (dotted) contours show southward winds. Contour interval is 0.5 m s^{-1}. This figure is available in colour online at wileyonlinelibrary.com/journal/qj

In any study of atmospheric heat transport, moist static energy is the natural variable to focus on (section 2.1). Furthermore, as we have established that spatial variability in h is set by the surface (and largely by SST), because h at upper levels is relatively uniform, we use the low-level moist static energy, h_{sfc}, as a basis to sort the mass transport in the atmosphere.

The dependence of mass transport on h_{sfc} means that we can visualize gross moist static stability in the atmosphere (the difference in moist static energy between upper and lower levels), as well as horizontal variations in moist static energy. Grouping regions of similar h_{sfc} together allows us to investigate the mean circulation present in different regions of the atmosphere, without the complication of geographical distribution. Values of relative humidity in the troposphere give an indication of the amount of atmospheric convection, and we include these in our analysis to show which regions of the tropics are likely to be convective, and what form the vertical structure of the mass transport takes in these regions.

3.2. *Method*

The lowest pressure level included in the ERA-40 dataset is 1000 hPa, which 'misses' the surface at the Equator where the pressure is often higher than 1000 hPa. A correction was thus made to the ERA-40 data to include mass fluxes in these regions by extrapolating the 1000 hPa variables to the surface. This means that we have redefined the lowest layer as extending from the surface pressure value to the pressure value halfway between 1000 hPa and the level above this (925 hPa).

The positive (northward) and negative (southward) mass transport (in kg s^{-1}) at the Equator, between the surface and 100 hPa for each degree longitude and for each pressure interval, is calculated as follows:

$$\delta\psi_{+} = v_{+}\frac{\delta P}{g}\delta x \tag{3}$$

$$\delta\psi_{-} = v_{-}\frac{\delta P}{g}\delta x \tag{4}$$

where, v_{+} is the northward meridional wind, v_{-} is the southward meridional wind and g is gravity. Next, the positive and negative mass transport as a function of longitude is binned depending on surface moist static energy, which is calculated as follows:

$$h_{\mathrm{sfc}} = C_{\mathrm{P}}T_{2\mathrm{m}} + L_{\mathrm{v}}q_{2\mathrm{m}} \tag{5}$$

where $T_{2\mathrm{m}}$ and $q_{2\mathrm{m}}$ are temperature and specific humidity taken at 2 m above the surface. Each h_{sfc} interval (bin) is equal to 1 K when divided by C_{P}. The positive and negative mass transport in each bin of h_{sfc} is then summed for each pressure interval and plotted as contours against h_{sfc} and pressure. Filled contours of the corresponding equatorial cross-section of tropospheric relative humidity are added as colours. For clarity and simplicity of interpretation, below we present in Figures 2, 3 and 5 the result of the mass transport/h_{sfc} analysis over the oceans only (around 80% of the data at the Equator), but will give the integrated transport over all grid points (ocean and land) for calculations included in the text.

Finally, note that throughout this analysis we use seasonal mean values for calculations of mass and heat transport for DJF and JJA. A calculation (not shown here) to quantify the eddy mean component of heat transport using daily data indicated that the daily component of heat transport at the Equator acted to enhance the cross-equatorial heat transport in JJA and DJF, but by only a small amount (<5% of the total seasonal mean heat transport). However, the eddy mean component of heat transport using daily data over a full year was not calculated.

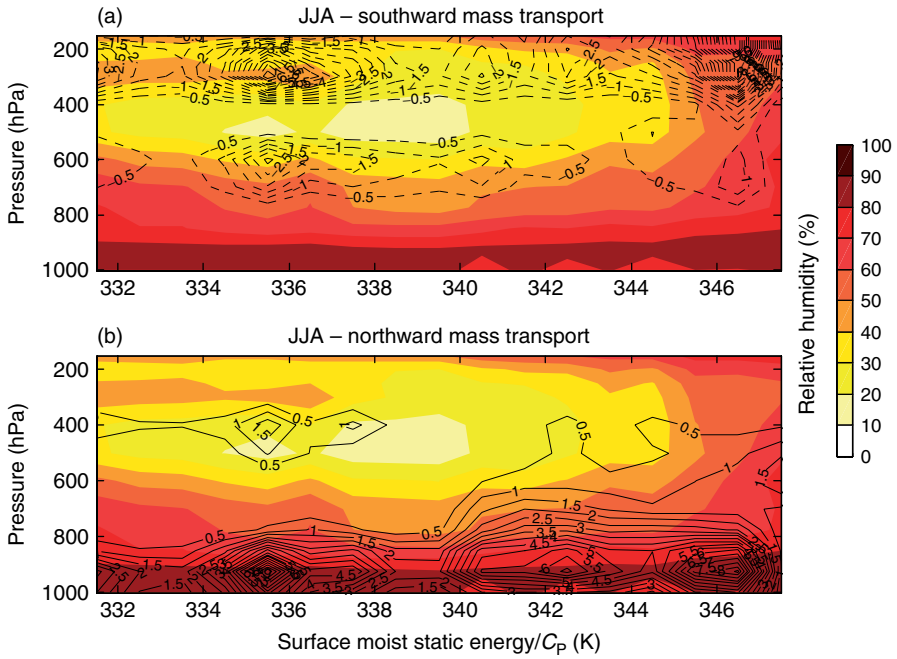

Figure 2. Relative humidity (shading: colours online) and mass transport (contours) at the Equator for JJA 1992–2001. Positive (solid) contours are summed northward mass transport for each pressure level (lower panel) and negative (dashed) contours are summed southward mass transport (upper panel), contour interval is 0.5 Sv. This figure is available in colour online at wileyonlinelibrary.com/journal/qj

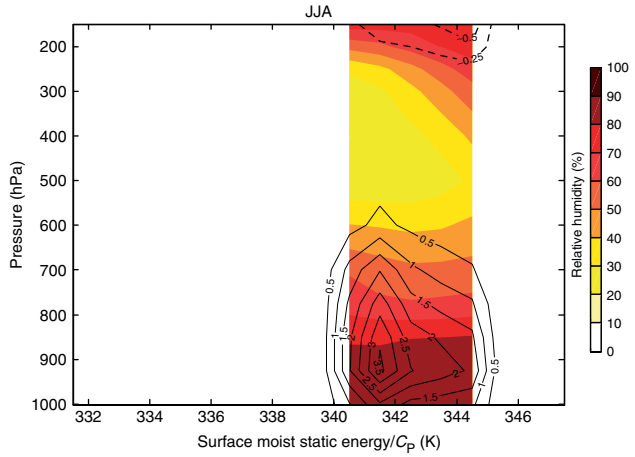

Figure 3. Positive and negative summed mass transport and relative humidity (as for Figure 2) for the region 40°–58° at the Equator, corresponding to the region of the Somali jet in JJA. This figure is available in colour online at wileyonlinelibrary.com/journal/qj

3.3. *Results*

The mass transport as a function of h_{sfc} for JJA is shown in Figure 2 and later for DJF in Figure 5 with southward mass transport in panel (a) and northward mass transport in panel (b). In those figures, shading (in colour online) shows relative humidity, solid contours are the sum of the positive (northward) mass transport and dashed contours are the sum of the negative (southward) mass transport. Again, the moist static energy (x-axis) has been divided by C_P so that the units are in Kelvin. Mass transport is in Sverdrups, and we use the Sverdrup as in Held (2001), where it is equal to 10^9 kg s^{-1}. The quantity represented by the contours in Figures 2, 3 and 5 (below) is summed mass transport for the corresponding value of surface moist static energy, and centred on each pressure level defined in section 2.2.

In the tropical oceans, the maximum SSTs do not vary greatly throughout the year, whereas the lowest SSTs (e.g. in the eastern Pacific) tend to vary much more from season to season (Peixoto and Oort, 1992), and this is reflected in h_{sfc}. For both seasons in the analysis, the maximum value of h_{sfc} is fairly constant at around 347 K, but the minimum value varies from 332 K in JJA to 338 K in DJF. For this reason, the minimum value on the x-axis scale varies in Figures 2 and 5 (below). In both seasons, high values of h_{sfc} (x-axis) correspond to high values of tropospheric relative humidity (shading: colour online), so that regions on the right-hand side of the plots can be considered to be frequently convecting. Towards the left-hand side of the plots are regions where h_{sfc} is low, such as the atmosphere over the eastern Pacific Ocean. In these regions, relative humidity is reduced and there is often a minimum at mid-tropospheric levels.

3.3.1. *June–August*

During JJA there is, in general, a northward transport of air across the Equator at low levels (continuous contours in Figure 2, bottom panel), and a southward return flow at upper levels (dashed contours in Figure 2, top panel). The centres of northward mass transport at low levels are approximately concentrated in three regions, corresponding to where values of h_{sfc} are around 335 K, 342 K and 346 K. These areas correspond to oceanic 'cold tongue' regions (eastern Pacific and Atlantic Ocean), the Somali jet and the Pacific and Indian Ocean warm pool, respectively.

The structure of the mass transport over the Indo-Pacific warm pool has a simple dipolar structure in the vertical, with most of the northward mass transport confined to areas below around 700 hPa and most of the southward mass transport confined to areas above around 500 hPa. Where this overturning circulation occurs, the relative humidity is high throughout the troposphere and weak vertical gradients

in moist static energy are seen, in agreement with the fact that convection occurs frequently over these regions. It is not clear at this stage whether this dipolar mass transport reflects the extension of equatorial overturning cells, convection being even more frequent at 10°–15°N and 5°S than at the Equator in JJA, or is a result of local convective processes at the Equator. The total northward mass transport for $h_{sfc} > 345.5$ K is found to be 43 Sv, while the total southward mass transport is 72 Sv for the same range of surface moist static energy (including atmosphere over ocean and land).

Over the cold tongue regions, values of h_{sfc} are low (around 335 K, Figure 2), implying that there is a larger moist static energy contrast between the upper level and the surface. A more complex vertical distribution of mass transport compared with the warmest regions is also clearly visible. There is northward mass transport at low levels and southward at upper levels, as expected, but also some southward mass transport centred around 700 hPa. There is weak northward transport at around 450 hPa in the colder regions. The low level return flow in these regions was also noted by Raymond *et al.* (2006) and Zhang *et al.* (2004), and could be due to suppressed convection as a result of descending air. As we are using monthly mean data, it is possible that in these regions there is a combination of deep convection and shallow convection on different time-scales, which are both reflected in the seasonal mean. The total northward transport in the range $h_{sfc} < 337.5$ is 78 Sv while it is 93 Sv for the total southward transport (again this is for ocean and land regions).

The northward transport centred at low levels on $h_{sfc} = 342$ K reflects the Somali jet, which is further studied in Figure 3, where the mass transport/h_{sfc} analysis is carried out only on the 40°–58° longitude sector. As in Figure 2, Figure 3 includes only oceanic regions, but mass transport calculations include both land and oceanic regions. The main feature observed is a jet-like structure from the surface to about 600 hPa, with a pronounced minimum in relative humidity above this layer. The total northward mass transport of the Somali jet is found to be 63 Sv, while the slight southward flow seen in Figure 3 amounts to 5 Sv. The northward mass transport by the Somali jet must thus be returned in a different longitudinal sector.

A schematic summary of the various mass transports discussed so far for JJA is given in Figure 4. The total northward transport across the Equator in JJA is found to be 294 Sv, while the total southward transport is 303 Sv. This reflects a small (3%) mass imbalance present in the ERA-40 dataset at that time of year.

3.3.2. *December–February*

During DJF, the vertical structure of the mass transport in the Indo-Pacific warm pool ($h_{sfc} \geqslant 344$ K) has a similar shape to that of JJA but is reversed in sign, so that the low level flow is southward and the upper level flow is northwards (Figure 5). Again, the relative humidity is high throughout the troposphere in this region. Note that some of the southward mass transport at low levels in this range of h_{sfc} is that due to the seasonal reversal of the southeast Asian monsoon flow (see Figure 1, top panel). The total northward and southward mass transport for the range $h_{sfc} > 345.5$ K is weaker than in JJA (36 Sv and 42 Sv, respectively, as opposed to 43 Sv and 72 Sv in JJA).

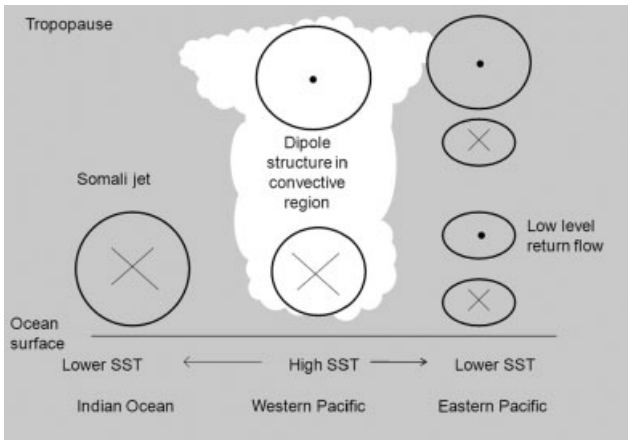

Figure 4. Schematic diagram representing features of mass transport over the Indian and Pacific oceans at the Equator in JJA. Circles and elipses represent centres of mass transport; crosses show circulation into the page (northward); dots represent transport out of the page (southward). The central region over the western Pacific is deeply convecting.

As in JJA, however, the cold tongue regions are singled out by their low level northward flow (339 K for the eastern Pacific and 343 K for the Atlantic), indicating that, unlike in the warmest regions, there is no seasonal reversal of the mass transport at low levels over the cold tongues. The vertical distribution of the mass transport over the latter region is as complex as it was in JJA, with southward flow below 600 hPa but an alternation of positive and negative flows above this level.

4. Heat transport

4.1. *Heat transport calculation*

Here we calculate the total cross equatorial poleward atmospheric heat transport as well as the heat transport associated with the regions where surface moist static energy is highest (the 'convective' regions) for DJF and JJA. The total northward heat transport (H_A) is computed using

$$H_A = \int_0^{2\pi R} \int_{P_{100}}^{P_{sfc}} vh \frac{dP}{g} dx \qquad (6)$$

in which v is the northward velocity, dx is the incremental distance along the equatorial circle of radius $2\pi R$ (R being the Earth's radius), and P_{100} refers to the 100 hPa pressure level. Note that unlike the mass transport calculations described in section 3, we have also corrected for the mass imbalance present in the ERA-40 dataset in order to compute H_A in Eq. (6). This was done by simply removing from each seasonal mean v its column (1000–100 hPa) averaged value.

We have identified a dipole structure of mass transport present in regions associated with high moist static energy and relative humidity, which is consistent with theoretical predictions by Emanuel *et al.* (1994). In order to calculate the heat transport, H_*, associated with this overturning circulation in the convecting regions of the tropics, we use a criterion based on vertical mean relative humidity and define convective regions as those where this value is >60%. On average the 60% relative humidity criterion means that around half the equatorial area is classed as 'convective'. Within these areas, a meridional overturning wind profile,

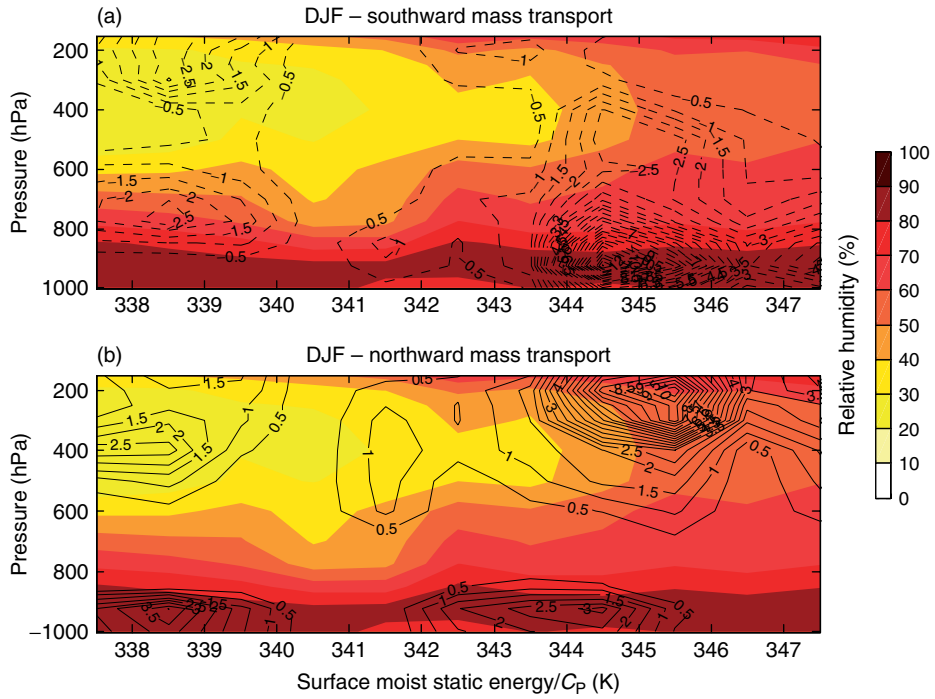

Figure 5. As for Figure 2 but for December through to February (DJF). This figure is available in colour online at wileyonlinelibrary.com/journal/qj

v_*, is obtained by removing the vertically averaged mean, that is:

$$v_* = v - \frac{1}{P_{\rm sfc} - P_{100}} \int_{\rm P_{100}}^{P_{\rm sfc}} v dP \qquad (7)$$

This meridional wind field is then used in conjunction with h to calculate H_* from

$$H_* = \tilde{L} \int_{\rm P_{100}}^{P_{\rm sfc}} v_* \tilde{h} \frac{dP}{g} \qquad (8)$$

in which $\tilde{L}$ is the longitudinal extent of the convective region based on the >60% relative humidity criterion and $\tilde{h}$ is the longitude-mean h profile at a given pressure level in the convective region. H_* represents the transport associated with a closed overturning circulation in the regions experiencing convection frequently, which can be compared with $H_{\rm A}$ to determine the relative importance of convective regions in atmospheric heat transport across the Equator. As mentioned in section 3.2, we use seasonal data because the contribution of subseasonal fluctuations in velocity and moist static energy to the cross-equatorial heat transport is negligible.

4.2. *The contribution of convective regions to the total atmospheric heat transport*

The distribution of moist static energy in Figure 1 shows a pronounced minimum in moist static energy at mid-levels (∼600 hPa). Over convective regions, Figures 2 and 5 furthermore indicate that this level roughly separates air parcels flowing northward and southward across the Equator. There is thus only a small contrast in moist static energy between these parcels with, as a rule of thumb, parcels at higher levels having the greater h. Indeed a calculation of mass weighted h above and below 600 hPa indicates values at upper levels larger by 3.5 K to 6.5 K depending on season (not shown). From these considerations southward heat transport over convective regions is thus expected in JJA, when the upper level mass transports are southward, and conversely, northward heat transport is expected in DJF, when upper level mass transports are northward. Application of Eq. (8) indeed confirms this expectation, with a comparable heat transport magnitude of $H_* \sim 1$ PW in both seasons (−1 PW in JJA, +0.94 PW in DJF).

Based on the 60% relative humidity criterion, the contribution from the convective regions in DJF is 80% of the total mean atmospheric heat transport, while it is 51% of the total mean atmospheric heat transport in JJA (see Table 1).

4.3. *The mean cross-equatorial heat transport*

Finally, we wish to come back to the issue of the net southward cross-equatorial heat transport that partly motivated this study. Application of Eq. (6) yields an annual atmospheric net heat transport at the Equator of −0.4 PW, that is, southward, which is consistent with Trenberth and Caron (2001) and Wunsch (2005). The annual mean value of H_*, based on regions above the 60% relative humidity threshold, however, is a net annual mean southward transport of only −0.1 PW. The bulk of the southward bias in annual mean atmospheric heat transport must thus be due to circulations other than the overturning seen in regions experiencing convection frequently.

A potential candidate is the monsoon circulation, highlighted in this study by the strong Somali jet in JJA (Figure 3). Relatively low moist static energy air is transported northward at low levels by the Somali jet while higher moist static energy air is returned southward at different longitudes and heights (as noted above, Figure 4 rules out a local return flow such as that occurring over the convective regions). During

Table 1. Seasonal mean calculations of total atmospheric (H_A) heat transport, convective region heat transport (H_*) and heat transported by the Somali jet (JJA and SON only). Heat transport by other regions is calculated as a residual

Season	Total mean heat transport (H_A) PW (% of total)	Convective region heat transport (H_*) PW (% of total)	Transport by Somali jet PW (% of total)	Transport by other regions (calculated as a residual) PW (% of total)
December–February	1.18 (100)	0.94 (80)	–	0.24 (20)
March–May	0.18 (100)	0.14 (78)	–	0.04 (22)
June–August	−1.98 (100)	−1.00 (51)	−0.60 (30)	−0.38 (19)
September–November	−0.86 (100)	−0.47 (55)	−0.20 (23)	−0.19 (22)

JJA, total cross-equatorial heat transport is around 2 PW, of which the convective region contributes about 1 PW. This leaves 1 PW accounted for outside the convective region. We can make an approximate calculation of the contribution by the southeast Asian monsoon circulation (associated with the Somali jet) by assuming a typical Somali jet mass transport of ∼60 Sv (section 3.3) and a moist static energy difference of around 10 K, which would account for a southward heat transport of ∼0.6 PW. (As mentioned in section 3.2, an even smaller contribution (∼0.03 PW) is accounted for by the eddy contribution to the seasonal total for JJA.) The Somali jet is also present, to a lesser extent, during the beginning of SON, and a similar calculation suggests a southward heat transport of ∼0.2 PW during this season. The mean seasonal heat transport and the relative contributions from the convective regions and the Somali jet (for JJA and SON only) are shown in Table 1. The final column represents heat transport that is not associated with the convective regions or the Somali jet, calculated as a residual (Table 1).

The contribution from the Somali jet, added to the 1 PW convective region contributions, explains around 81% of the total atmospheric heat transport during JJA (number in parenthesis in Table 1). During SON, the corresponding figure is 78%. These figures can be compared with DJF, when the Somali jet is not present, and the convective region accounts for around 80% of the total DJF transport. Note that the residual heat transport (that not accounted for by the Somali jet or the convective regions) varies very little between seasons (ranging from 19 to 22% of the total heat transport). The greatest southward heat transport across the Equator occurs during JJA, and as we have seen that the Somali jet contributes up to ∼0.6 PW of the 2 PW total in JJA (and a further ∼0.2 PW of the 0.86 PW total in SON), it is reasonable to suggest that the Somali jet is a significant contributor to the annual southward asymmetry in atmospheric heat transport at the Equator. Indeed, integrating the heat transport over a year using the numbers in Table 1 yields a net 0.37 PW or 1.17×10^{22} J carried south across the Equator annually, of which approximately 26% is due to motions in convective regions, 54% by the Somali jet and 20% by motions other than the previous two (the residual).

This conclusion is only tentative considering that the annual mean heat transports discussed here are not much larger than typical errors (∼0.1 PW) quoted in the literature (e.g. Trenberth and Caron, 2011). In addition, a proper Lagrangian analysis is required to set the moist static energy difference involved in the heat transport by the monsoon circulations. Nevertheless, the impact of the Somali jet on the cross-equatorial heat budget is an interesting feature of the ERA-40 dataset, because it shifts the focus away from the cold tongue regions, which are often invoked to explain north–south asymmetry in the climatology (e.g. Mitchell and Wallace, 1992). To rationalize why the cold tongue regions might not play such a large role in mean southward heat transport across the Equator, consider the following. The cold tongue circulations were highlighted in Figures 2 and 5 by a well-defined northward 'jet' below 850 hPa ($h_{sfc} < 339$ K in JJA and $h_{sfc} < 344$ K in DJF). For them to produce an annual mean southward heat transport, this 'jet' must be at a lower h than its associated southward return flow. Considering that the cold tongue regions have the lowest h_{sfc} in all seasons, this seems at first sight to be a real possibility. However, the complexity of the mass transport over low h_{sfc} regions, emphasized in section 3, does not rule out that a significant fraction of the northward mass transport is returned locally at mid-levels where moist static energy is actually lower than that at the surface – see for example Figures 2a and 5a over the $h_{sfc} \leqslant 340$ K region.

5. Conclusions

The analysis of atmospheric heat transport presented in this study has highlighted at least three different types of circulation that might ultimately set up what is usually referred to as 'heat transport by the Hadley cell' at low latitudes. Over warm and moist regions of the tropics, a deep overturning cell is observed with southward and northward flows at lower and upper levels approximately in balance over the longitudinal extent of these regions. The moist static energy contrast between these flows is small but the mass transport is sufficiently large to contribute significantly to the seasonal mean cross-equatorial heat transport. A more three-dimensional, 'gyre-like'* structure of the heat transport is offered by the southeast Asian monsoon circulation, where the low level northward flow of low moist static energy air in the Somali jet feeds the southeast Asian monsoon and is eventually transformed into a higher moist static energy air mass and returned southward thereafter. Finally, over the cold tongues of the equatorial Pacific and Atlantic oceans, an even more intricate distribution of the meridional mass transport is seen, with northward and southward flow alternating in the vertical in a quadrupolar fashion.

From these results, the apparent dominance of axisymmetric mechanisms to transport heat at low latitudes can be rationalized as follows. The initial working hypothesis, namely that the deep overturning cells found in regions experiencing frequent convection would dominate the poleward heat transport, provides a simple description for a given season. However, due to a strong seasonal cancellation, it

*This terminology is not too strong considering that the Somali jet has been proposed as an atmospheric analogue to the Gulf Stream (R. Hide, personal communication; Anderson, 1976).

must be rejected for the annual mean, especially at the Equator. Indeed, the calculations above suggest that the deep overturning cells found in regions experiencing frequent convection account only for about 25% of the mean cross-equatorial heat transport. It is thus proposed that the Monsoon circulation plays a significant role in southward cross-equatorial heat transport and that it displays a deep overturning circulation in the zonal mean since, plausibly, the return flow of the Somali jet occurs at upper levels. Very little contribution to year round poleward heat transport is suggested for the cold tongue-induced circulations because of their complex meridional mass transport profiles and the pronounced minimum in moist static energy at mid-levels.

The fact that the atmosphere carries heat southward across the Equator in the mean, partly as a result of the asymmetry in the monsoonal circulation, as suggested here, rather than as a result of the presence of ITCZ north of the Equator year round over the eastern Pacific and Atlantic oceans, puts a fresh perspective on the observed compensation between oceanic and atmospheric cross-equatorial heat transport. Indeed, on the oceanic side, cross-equatorial heat transport is attributed to the thermohaline component of the circulation (Rahmstorf, 1996). Gupta *et al.* (2003) identified a link between cold periods in the North Atlantic region and the Indian Ocean monsoon using palaeoclimate techniques and suggested that possible mechanisms could be due to variations in solar output or internal forcing caused by oscillations in North Atlantic heat transport and deep-water production. This relationship was modelled by Zhang and Delworth (2005), who simulated a reduction in the thermohaline circulation and observed a corresponding southward shift of the ITCZ, an El Niño-like pattern in the Pacific and weakened Indian and Asian summer monsoons due to air–sea interactions. More recently, Lu and Dong (2008) noted a correlation between a weakened North Atlantic circulation and a suppressed Asian summer monsoon, which they explained by the atmospheric teleconnection in the eastern and central North Pacific, as well as atmosphere–ocean interaction in the tropical North Pacific. These studies are consistent with the idea of compensation highlighted here, because a weaker oceanic overturning, leading to a smaller northward oceanic heat transport, is found to be associated with a weaker monsoon, and thus a weaker southward annual atmospheric heat transport. Understanding how the thermohaline circulation interacts with the monsoon is an intriguing and exciting challenge that deserves further study.

Acknowledgements

This study is part of C. Heaviside's PhD funded by the Natural Environment Research Council. The authors would like to thank the two anonymous reviewers for their thoughtful and detailed feedback, which was very helpful in the preparation of this article.

References

Anderson DLT. 1976. The low level jet as a western boundary current. *Mon. Weather Rev.* **104**: 907–921.

Bohren CF, Albrecht BA. 1998. *Atmospheric Thermodynamics*. Oxford University Press: Oxford.

Bony S, Dufresne JL, Le Treut H, Morcrette JJ, Senior C. 2004. On dynamic and thermodynamic components of cloud changes. *Clim. Dynam.* **22**(2–3): 71–86.

Czaja A, Marshall J. 2006. Partitioning of poleward heat transport between the atmosphere and ocean. *J. Atmos. Sci.* **63**(5): 1498–1511.

Dima IM, Wallace JM. 2003. On the seasonality of the Hadley cell. *J. Atmos. Sci.* **60**(12): 1522–1527.

Emanuel KA, Neelin JD, Bretherton CS. 1994. On large-scale circulations in convecting atmospheres. *Q. J. R. Meteorol. Soc.* **120**(519): 1111–1143.

Gill AE. 1980. Some simple solutions for heat-induced tropical circulation. *Q. J. R. Meteorol. Soc.* **106**(449): 447–462.

Gill AE. 1982. *Atmosphere–Ocean Dynamics*, 1st edn. Academic Press.

Gupta AK, Anderson DM, Overpeck JT. 2003. Abrupt changes in the Asian southwest monsoon during the holocene and their links to the North Alantic Ocean. *Nature* **421**(6921): 354–357.

Held IM. 2001. The partitioning of the poleward energy transport between the tropical ocean and atmosphere. *J. Atmos. Sci.* **58**(8): 943–948.

Held IM, Schneider T. 1999. The surface branch of the zonally averaged mass transport circulation in the troposphere. *J. Atmos. Sci.* **56**(11): 1688–1697.

Lu R, Dong B. 2008. Response of the Asian summer monsoon to weakening of Atlantic thermohaline circulation. *Adv. Atmos. Sci.* **25**(5): 723–736.

Mitchell TP, Wallace JM. 1992. The annual cycle in equatorial convection and sea-surface temperature. *J. Climate* **5**(10): 1140–1156.

Neelin JD, Held IM. 1987. Modeling tropical convergence based on the moist static energy budget. *Mon. Weather Rev.* **115**(1): 3–12.

Oort AH, Yienger JJ. 1996. Observed interannual variability in the Hadley circulation and its connection to ENSO. *J. Climate* **9**(11): 2751–2767.

Pauluis O, Czaja A, Korty R. 2008. The global atmospheric circulation on moist isentropes. *Science* **321**(5892): 1075–1078.

Peixoto JP, Oort AH. 1992. *Physics of Climate*. American Institute of Physics: New York.

Philander SG. 1990. *El Nino, La Nina and the Southern Oscillation*. Academic Press.

Philander SGH, Gu D, Halpern D, Lambert G, Lau NC, Li T, Pacanowski RC. 1996. Why the ITCZ is mostly north of the equator. *J. Climate* **9**(12): 2958–2972.

Polvani LM, Sobel AH. 2002. The Hadley circulation and the weak temperature gradient approximation. *J. Atmos. Sci.* **59**(10): 1744–1752.

Rahmstorf S. 1996. On the freshwater forcing and transport of the Atlantic thermohaline circulation. *Clim. Dynam.* **12**(12): 799–811.

Raymond DJ, Bretherton CS, Molinari J. 2006. Dynamics of the intertropical convergence zone of the east Pacific. *J. Atmos. Sci.* **63**(2): 582–597.

Trenberth KE, Caron JM. 2001. Estimates of meridional atmosphere and ocean heat transports. *J.Climate* **14**(16): 3433–3443.

Trenberth KE, Stepaniak DP, Hurrell JW, Fiorino M. 2001. Quality of reanalyses in the Tropics. *J. Climate* **14**(7): 1499–1510.

Uppala SM, Kållberg PW, Simmons AJ, Andrae U, da Costa Bechtold V, Fiorino M, Gibson JK, Haseler J, Hernandez A, Kelly GA, Li X, Onogi K, Saarinen S, Sokka N, Allan RP, Andersson E, Arpe K, Balmaseda MA, Beljaars ACM, van de Berg L, Bidlot J, Bormann N, Caires S, Chevallier F, Dethof A, Dragosavac M, Fisher M, Fuentes M, Hagemann S, Hólm E, Hoskins BJ, Isaksen L, Janssen PAEM, Jenne R, McNally AP, Mahfouf JF, Morcrette JJ, Rayner NA, Saunders RW, Simon P, Sterl A, Trenberth KE, Untch A, Vasiljevic D, Viterbo P, Woollen J. 2005. The ERA-40 reanalysis. *Q. J. R. Meteorol. Soc.* **131**(612): 2961–3012.

Wallace JM. 1992. Effect of deep convection on the regulation of tropical sea-surface temperature. *Nature* **357**(6375): 230–231.

Wunsch C. 2005. The total meridional heat flux and its oceanic and atmospheric partition. *J. Climate* **18**(21): 4374–4380.

Xu K-M, Emanuel KA. 1989. Is the tropical atmosphere conditionally unstable? *Mon. Weather Rev.* **117**(7): 1471–1479.

Zhang CD, McGauley M, Bond NA. 2004. Shallow meridional circulation in the tropical eastern Pacific. *J. Climate* **17**(1): 133–139.

Zhang R, Delworth TL. 2005. Simulated tropical response to a substantial weakening of the Atlantic thermohaline circulation. *J. Climate* **18**(12): 1853–1860.

